JOURNAL OF GEOPHYSICAL RESEARCH, VOL. 115, D04203, doi:10.1029/2009JD012219, 2010

Global increase in UV irradiance during the past 30 years (1979–2008) estimated from satellite data

Jay R. Herman[1]

Received 8 April 2009; revised 18 September 2009; accepted 25 September 2009; published 25 February 2010.

[1] Zonal average ultraviolet irradiance (flux ultraviolet, F_{UV}) reaching the Earth's surface has significantly increased since 1979 at all latitudes except the equatorial zone. Changes are estimated in zonal average F_{UV} caused by ozone and cloud plus aerosol reflectivity using an approach based on Beer's law for monochromatic and action spectrum weighted irradiances. For four different cases, it is shown that Beer's Law leads to a power law form similar to that applied to erythemal action spectrum weighted irradiances. Zonal and annual average increases in F_{UV} were caused by decreases in ozone amount from 1979 to 1998. After 1998, midlatitude annual average ozone amounts and UV irradiance levels have been approximately constant. In the Southern Hemisphere, zonal and annual average UV increase is partially offset by tropospheric cloud and aerosol transmission decreases (hemispherical dimming), and to a lesser extent in the Northern Hemisphere. Ozone and 340 nm reflectivity changes have been obtained from multiple joined satellite time series from 1978 to 2008. The largest zonal average increases in F_{UV} have occurred in the Southern Hemisphere. For clear-sky conditions at 50°S, zonal average F_{UV} changes are estimated (305 nm, 23%; erythemal, 8.5%; 310 nm, 10%; vitamin D production, 12%). These are larger than at 50°N (305 nm, 9%; erythemal, 4%; 310 nm, 4%; vitamin D production, 6%). At the latitude of Buenos Aires, Argentina (34.6°S), the clear-sky F_{UV} increases are comparable to the increases near Washington, D. C. (38.9°N): 305 nm, 9% and 7%; erythemal, 6% and 4%; and vitamin D production, 7% and 5%, respectively.

Citation: Herman, J. R. (2010), Global increase in UV irradiance during the past 30 years (1979–2008) estimated from satellite data, *J. Geophys. Res.*, *115*, D04203, doi:10.1029/2009JD012219.

1. Introduction

[2] Changes in the amount of UVB (280–315 nm) and short wavelength UVA (315–325 nm) irradiances that reach the earth's surface are dependent on changes in the amounts of ozone (O_3), aerosol, and cloud albedo. Changes in aerosol and cloud albedo also affect UVA (315–400 nm), VIS (400–700 nm), and NIR (700–2000 nm). From the viewpoint of exposure (time integral of irradiance from sunrise to sunset) to UV, very high clear-sky UV irradiances F_{UV} and exposures E_{UV} occur in tropic latitudes, ±23.3°, following the seasonal subsolar point, also at high mountain altitudes and occasionally when the elongated ozone hole passes over southern Chile and Argentina. In general, UV erythemal, UV-A, and UV-B irradiances decrease with increasing latitude outside of the equatorial zone, due to the decreases in maximum daily noon solar elevation angles and increases in ozone amount with increasing latitude. At the equator, larger UV monthly average irradiance exposure occurs when the Sun is directly overhead during March equinox conditions, which has lower cloud cover than during September. The difference is related to the annual cycle of the cloud cover associated with the Intertropical Convergence Zone (ITCZ), which is usually over the equator in September, but is south of the equator in March. Two examples of very high E_{UV} occur in the South American Andes (e.g., the sparsely populated Atacama Desert in Chile at 4400 m to 5600 m altitude and in the city Cuzco, Peru 13.5°S, 72°W) during January (noon solar zenith angle SZA = 9.5°) and in the Himalayan Mountains during July (over 100 peaks exceeding 7000 m with Everest at 28°N, 27°E, SZA = 5.5°). In both cases, the summer Sun is nearly overhead.

[3] In January the Earth's elliptical orbit is closest to the Sun (perihelion near January 3) compared to the Northern Hemisphere (NH) summer (aphelion near 4 July) causing a 6% increase in Southern Hemisphere (SH) irradiance at the top of the atmosphere around perihelion compared to the NH near aphelion.

[4] Based on the combined multisatellite ozone data set used in this paper [*Stolarski and Frith*, 2006], average summer ozone in the midlatitude SH (30°S–50°S) (December 2007; 288 DU) is lower than at corresponding latitudes in the NH (June 2008; 305 DU) by about 6%, which contributes to higher summer clear-sky UVB irradiances in the SH. The exact percentage of ozone interhemispheric difference is a function of latitude, longitude, year, and season. In

[1]NASA Goddard Space Flight Center, Greenbelt, Maryland, USA.

Table 1. Satellite Instruments for Ozone and Reflectivity

Years	Instrument	Details
1979–1992	Nimbus-7/TOMS (N7)	Full global coverage every day. Only a few missing days from 1980 to 1992. Ozone plus reflectivity. Near noon orbit
1985–2008[a]	SBUV-2 Series (N-9, N-11, N-16, N-17, N-18)	Nadir viewing only. Only a few missing days. Ozone plus reflectivity. N-9 and N-11 have a drifting orbit.
1996–2006	Earth-Probe/TOMS (EP)	Full global coverage every day. Only a few missing days in 10 years. The calibration precision was improved by using N-16 as a reference. Not used for cloud plus aerosol reflectivity. Near noon orbit.
1997–2008[a]	SeaWiFS (SW)	The 412 nm reflectivity has been produced using the TOMS production algorithm. Does not measure ozone. Noon orbit.
2004–2008[a]	Ozone Monitoring Instrument (OMI)	Full global coverage every day with few missing days. OMI produces both ozone and reflectivity values. 1:30 PM orbit.

[a]Satellites are still obtaining data as of mid-2009.

general, the SH has fewer pollution aerosols, which leads to less reduction in F_{UV} reaching the surface relative to NH aerosol pollution effects. Exceptions occur in regions with intense seasonal biomass burning (e.g., southern Africa and central Brazil).

[5] Global estimates of long-term F_{UV} change from satellite ozone and reflectivity data were previously discussed using observations from Nimbus-7 Total Ozone Mapping Spectrometer (N7-TOMS) for the period 1979 to 1992 [*Herman et al.*, 1996], and corresponded to papers on long-term ozone change [*Stolarski et al.*, 1991; *Gleason et al.*, 1993, *Herman et al.*, 1999; *McKenzie et al.*, 2001; *Fioletov et al.*, 2001, 2002]. A number of studies have discussed the validation of satellite estimates of F_{UV} in comparison to ground-based measurements [e.g., *Herman et al.*, 1999; *Krotkov et al.*, 1998, 2001; *Tanskanen et al.*, 2007; *Kalliskota et al.*, 2000]. The basic conclusion of these studies is that satellite estimates of F_{UV} are within a few percent of ground-based measurements for nonmountainous, snow-free, clear-sky, low-pollution sites. Even for clear skies, absorbing aerosols over a polluted urban environment typically cause F_{UV} estimates from satellite radiance data to overestimate by 10% to 15% and occasionally by as much as 40% [*Kalliskota et al.*, 2000; *McKenzie et al.*, 2001; *Fioletov et al.*, 2004]. Large differences, up to 40%, have been observed in mountain areas. This study only discusses zonal average F_{UV} in 5° latitude bands, where the influence of polluted urban sites and mountainous terrain is minimized.

[6] Long-term changes in ozone amount have been discussed at length in several recent World Meteorological Organization reports [*World Meteorological Organization (WMO)*, 1999, 2003, 2007], which summarize the ozone data obtained by both ground-based and satellite measurements. The basic conclusions for ozone in the latest report [*WMO*, 2007] are: (1) Ozone has decreased since 1979 in Northern Hemisphere (NH) and Southern Hemisphere (SH) high and middle latitudes, but the decreases have leveled off during the past several years with some indications of recovery. (2) There have been no significant trends in ozone amount for low latitudes between about 25°S and 25°N. (3) Current ozone values are still below the amounts measured in 1979–1980 at middle and high latitudes.

[7] Global estimations of the amount of ozone and cloud plus aerosol reflectivity have been obtained from a series of satellite instruments that are summarized in Table 1.

[8] The Nimbus-7 Total Ozone Mapping Spectrometer (TOMS) measures six radiance channels with nominal wavelengths 312.3, 317.4, 331.1, 339.7, 360.0, and 380.0 nm, of which the first three are sensitive to ozone and the second three are insensitive to ozone. The latter are used for scene reflectivity measurements, which are needed for ozone amount retrieval and for determining the amount of cloud transmission used for estimating the UV irradiance reaching the ground. EP-TOMS has the following wavelengths, 308.6, 313.5, 317.5, 322.3, 331.2, and 360.44 nm, with only the 360 nm channel insensitive to ozone.

[9] The SBUV (Solar Backscatter Ultra Violet) series have more wavelength channels, 256, 273, 283, 288, 292, 298, 302, 306, 312, 318, 331, and 340 nm, with only one channel, 340 nm insensitive to ozone. SeaWiFS is an 8 channel instrument with relatively wide filter wavelength band passes 402–422, 433–453, 480–500, 500–520, 545–565, 660–680, 745–785, 845–885 nm, where the first channel 402–422, is labeled by its center wavelength 412 nm. The 412 nm channel most closely resembles the UV reflectivity wavelengths in that the surface reflectivity is only a few RU (1 RU = 0.01 or 1% reflectivity) and is almost independent of changes in vegetation. OMI measures from 270 to 500 nm with a spectral resolution from 0.45 nm to 0.65 nm [*Levelt et al.*, 2006]. Each of these instruments measures radiances with different ground resolution ranging from about 200 × 200 km^2 for SBUV to 4 km^2 (nadir) for SeaWiFS. Because of the disparity in resolution and global coverage between the different instruments, only zonal averages are used in 5° latitude bands (at low latitudes, 1° of latitude is approximately 100 km).

[10] The ozone data were obtained from NASA Goddard Space Flight Center's website (http://hyperion.gsfc.nasa.gov/Data_services/merged/index.html) for monthly and 5° zonal average band values. The combined multisatellite ozone data set and computed trends are described by *Stolarski and Frith* [2006]. Reflectivity data are available from the same website, and are described in a recent paper [*Herman et al.*, 2009]. The combined multisatellite reflectivity data set is formed from the arithmetic average of overlapping data from N7, SBUV-2 series, and OMI. SW is not used in this study, since the relation between 412 nm reflectivity and 340 nm reflectivity has not yet been adequately established. EP is not used for long-term reflectivity studies, since its calibration has been normalized to N-16, but still contains some obvious radiance calibration drifts, especially at high latitudes. Reflectivity is more sensitive to instrument calibration drifts, since it is estimated from single wavelength radiance measurements, whereas

ozone is mostly derived from ratios of two or more wavelengths, which cancels some errors. The latitude range in this study is limited to 55°S to 55°N to avoid high solar zenith angle effects and seasonal bias caused by missing data during polar nights.

[11] This paper estimates F_{UV} changes that have occurred during 30 years from 1979 to 2008 for both monochromatic and four action spectrum weighted irradiances based on Beer's Law radiative transfer and the Radiation Amplification Factor (RAF) concept. It is shown that the RAF power law method of estimating action spectrum weighted F_{UV} changes can be derived directly from the exponential form of Beer's Law for a wide range of ozone values (200 to 600 DU) and for four different action spectra.

2. Estimating Irradiance Changes

[12] The inverse relation between ozone changes and UVB irradiance changes is well established by both theory and measurements. For example, earlier work done by *Latarjet* [1935] and *Bener* [1972] provided the basis for deriving semiempirical relations between ozone and UVB irradiance. A more recent work [*Micheletti et al.*, 2003] extended the analysis to derive a power law form relating ozone change to a special case of action spectra weighted irradiance change. A convincing set of erythemal weighted irradiance P_{ERY} versus ozone amount measurements were obtained during July 1995 to July 1996 at Mauna Loa Observatory (19.5°N, 155.6°W, 3.4 km altitude) for 132 clear mornings with a solar zenith angle SZA = 45° [*Bodhaine et al.*, 1997; *WMO*, 1999]. The measured result as a function of ozone amount Ω was an almost perfect inverse power law relationship ($P/P_{REFERENCE} = (\Omega/\Omega_{REFERENCE})^{-RAF(SZA)}$) with a measured exponent of about RAF = −1.38 for an average Ω of about 250 DU. A series of erythemal irradiance measurements were made at Mauna Loa Observatory as a function of solar zenith angle SZA to determine RAF(SZA). For small SZA = 20°, RAF = 1.28, and rose to about 1.38 for SZA = 35° to 60°, and decreased rapidly for higher SZA [*Bodhaine et al.*, 1997]. According to Bodhaine et al., the change from 1.28 to 1.38 was not considered to be statistically significant.

[13] A similar result was obtained for monochromatic irradiances $F(\lambda)$ as a function of wavelength λ from 295 nm to 340 nm that matched the predictions obtained with the radiation amplification factor RAF [*Madronich*, 1993] using the form $dF(\lambda)/F(\lambda) = -RAF(\lambda, \Omega)\, d\Omega/\Omega$ (e.g., RAF(305) = 2.05 and RAF(310) = 1.06 for a 1% decrease in Ω), where $RAF = \alpha\Omega\sec(\theta)$, Ω = ozone column amount in Dobson Units (1 DU = 1 milli-atm-cm or 2.69×10^{16} molecules/cm^2), α = ozone absorption coefficient (in cm^{-1}), θ = solar zenith angle SZA.

[14] There are two common forms using the RAF concept for estimating changes in irradiance caused by changes in ozone amount that avoid the need for numerical solutions to a radiative transfer equation that includes multiple scattering. The first form is based on Beer's Law for monochromatic transmission through an absorbing atmosphere (ozone) with scattering neglected.

$$(F_1\text{-}F_2)/F_2 = \exp[-\alpha\Omega_2\sec(\theta)(\Omega_1 - \Omega_2)/\Omega_2] - 1. \quad (1)$$

The second is based on an apparently empirical Power Law, which can be used to model the changes in action spectrum weighted irradiance functions over a range of wavelengths caused by changes in ozone amount. The Power Law form (equation (2)) matches measured broadband erythemal irradiance data quite well [*Booth and Madronich*, 1994; *Blumthaler et al.*, 1995; *Bodhaine et al.*, 1997].

$$F_1/F_2 = (\Omega_1/\Omega_2)^{-RAF(\theta)} \text{ or}$$
$$(F_1\text{-}F_2)/F_2 = [1 + (\Omega_1 - \Omega_2)/\Omega_2]^{-RAF(\theta)} - 1. \quad (2)$$

For small changes in ozone amount, the two forms yield approximately the same value for $dF_{12}/F_2 = (F_1 - F_2)/F_2$. Later it is shown that the results for broadband irradiance changes (equation (2)) can be obtained by wavelength integration using equation (1).

3. Ozone Changes

[15] The long-term (30 year) monthly and zonal average (5° bands) ozone time series can be used to estimate the change in ozone $d\Omega$ causing a fractional change in irradiance dF_{12}/F_2 reaching the earth's surface. The percent changes in ozone amount over 30 years are calculated directly from the zonal and monthly average merged ozone time series described by *Stolarski and Frith* [2006] with the reference ozone value taken as the 1979 annual average for each latitude band. As an example using equation (1), the results for 305 nm dF_{12}/F_2, relative to the 1979 annual average 305 nm F_2, are shown in Figure 1 for latitude bands centered on 32.5°S and 32.5°N. The ozone percent change $d\Omega_{12}/\Omega_2$ is about 100*30*(−0.37)/294 = −3.8% at 32.5°S and 100*30*(−0.3)/300 = −3% at 32.5°N over 30 years. The clear-sky increase in 305 nm irradiance dF_{12}/F_2 is about 6.3 ± 2% at 32.5°S and 5.4 ± 2% at 32.5°N over 30 years for the summer months centered on solstice.

[16] The two factors contributing to the clear-sky 305 nm irradiance changes in Figure 1 are the seasonal changes in $\sec(\theta)$ and Ω. The red circles in Figure 1 mark the respective summer solstices and the blue squares mark the winter solstices. This shows that the summer increases in F approximately follows the annual mean increase represented by the least squares fit line to the dF_{12}/F_2 time series. By the end of 30 years the summertime 305 nm irradiance increased by about 6 ± 2% in both hemispheres at 32.5° latitude. The change in irradiance is not a simple linear function of time, since the increase in June 305 nm irradiance levels off in about 1998 at 32.5°N and about in 1994 for 32.5°S. While 6% is a significant increase in 305 nm irradiance, further increases may not occur in the future, since it appears that the decrease in ozone and the corresponding increase in irradiance have leveled off starting in the middle 1990s. This is likely to have been a direct result of adherence to the 1989 Montreal Protocol, and subsequent agreements (1990, 1991, 1992, 1993, 1995, 1997, and 1999) limiting the injection chlorine and bromine bearing compounds into the atmosphere. A model estimate of irradiance changes that might occur in the absence of these agreements is given by *Newman et al.* [2009].

[17] The nonlinear trend in winter values at 32.5°N starts out with a larger rate of increase (0.006/year) until 1996,

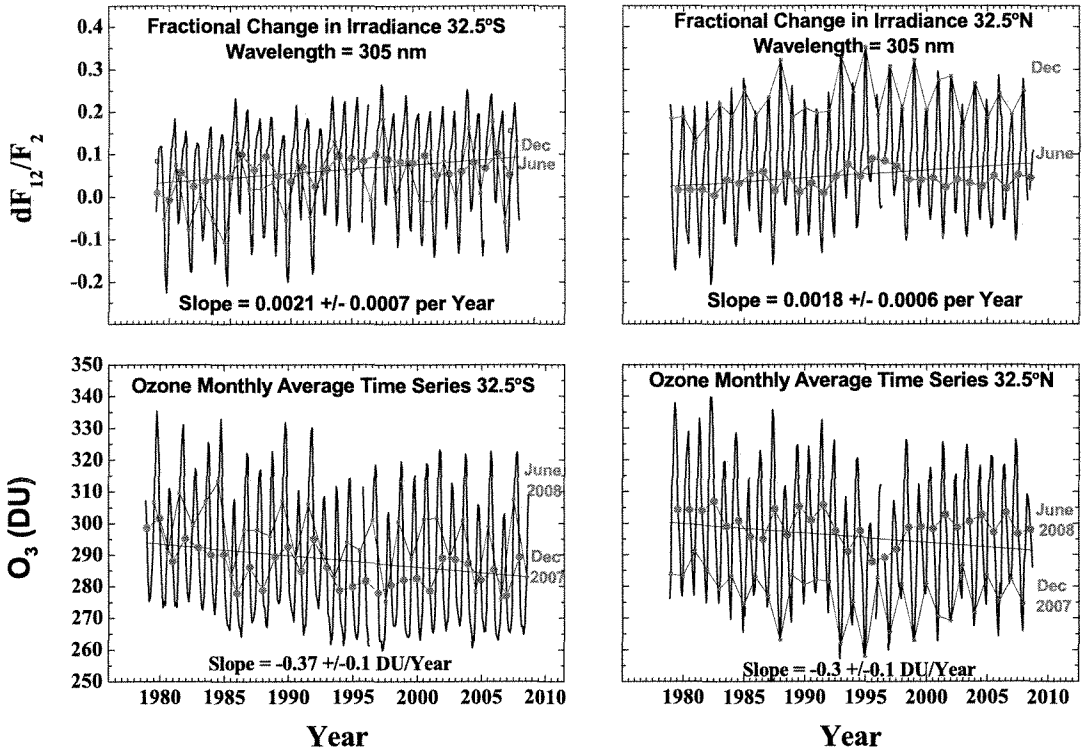

Figure 1. (top) Fractional change in 305 nm irradiance dF_{12}/F_2 caused by (bottom) a change in ozone and SZA in two latitude bands centered on (left) 32.5°S and (right) 32.5°N of 5° width. The red circles are the summer solstice months of December (−32.5°S) and June (32.5°N), and the small blue squares are the winter solstice months. The monthly average ozone values are from the GSFC website based on merged data from multiple satellites. http://hyperion.gsfc.nasa.gov/Data_services/merged/index.html.

and then decreases (−0.005/year) between 1996 and 2008. Bilinear trends can be estimated using a Fourier transform low-pass filter on the time series data to estimate the date of the inflection point. The estimated inflection point date can be used as the intermediate endpoint between the two linear trend sections of data. At 32.5°S, the winter values increase at a rate of 0.005/year until 1996, after which the slope is not significantly different than zero.

[18] Similar analysis can be performed for all wavelengths and latitude bands between 55°S and 55°N including the effect of cloud plus aerosol and ozone changes. The 305 nm wavelength has been chosen as an example because of its sensitivity to ozone change and its importance in detrimental skin effects and beneficial vitamin D production.

4. Reflectivity Changes From Clouds and Aerosols

[19] The presence of clouds and aerosols in a satellite observed scene increases the amount of radiation reflected back to space and decreases the amount reaching the ground. Changes in Lambert Equivalent Reflectivity have been described in previous studies based on Nimbus-7 TOMS and SeaWiFS observations for the separate periods 1980 to 1992 and 1998 to 2006 [*Herman et al.*, 1996, 1999, 2009]. Examples of the 30 year zonal average reflectivity time series are shown in Figure 2, which are derived from numerically averaging the overlapping time series from the Nimbus-7/TOMS and SBUV-2 satellites. All of these satellite data sets are based on in-flight recalibration using the Antarctic and Greenland ice sheets as calibration references. Details of the satellite recalibrations used to estimate the zonal average and latitude by longitude reflectivity data sets will be presented in a future paper.

[20] The largest changes in zonal average reflectivity occur in the SH between 20°S and 60°S. Figure 2 shows four typical reflectivity time series samples centered on 17.5°S, 17.5°N, 42.5°S, and 42.5°N based on daily data (light gray). Superimposed on the daily data are estimates of 30 year linear least squares fits to the data.

[21] The SH reflectivity data shows a long-term increase starting at about 27.5°S, with the largest changes occurring at higher latitudes. However, the increase in reflectivity occurred in the early portion of the time series and leveled off or even slightly decreased in the later portions. For example, at 42.5°S (Figure 2c), the 1979 to 1992 slope S of the linear least squares fit is S = 0.16 ± 0.02 RU per year and for the period 1998 to 2008 S = 0.05 ± 0.01 RU/year. The leveling off in reflectivity change reduces the long-term 1979 to 2008 linear change to S = 0.06 ± 0.005 RU/year. Similar bimodal linear slopes occur for all SH latitudes greater than 27.5°S. This is similar to the pyranometer results from *Liley* [2009], which found that there was an

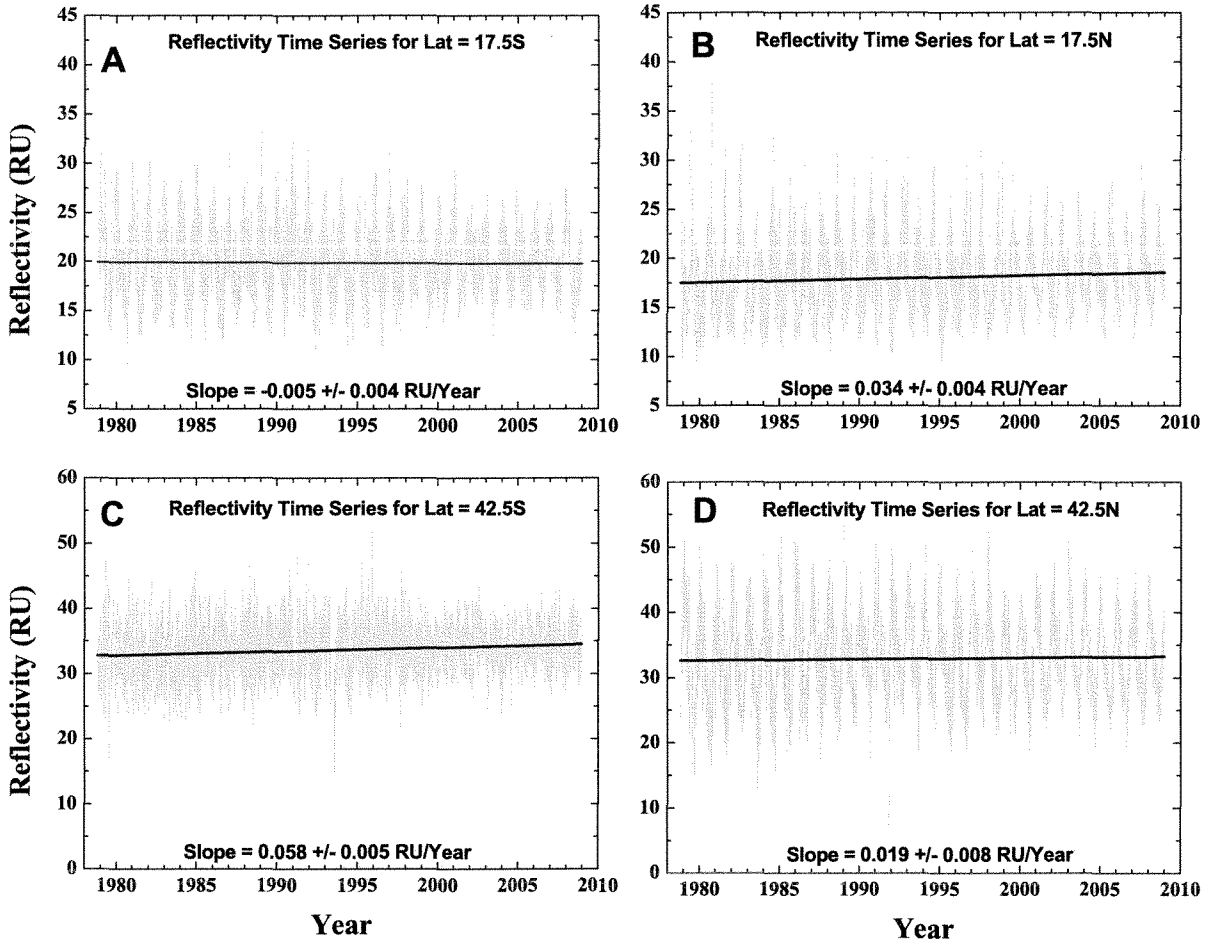

Figure 2. Reflectivity time series 1979 to 2008 for 5° latitude bands centered at (a) 17.5°S and (b) 17.5°N and (c) 42.5°S and (d) 42.5°N. The units are RU (1 RU = a reflectivity of 0.01 or 1%). The straight lines are linear least squares fits to the entire data set.

increase in cloud cover over New Zealand until 1990 and a decline after 1990.

[22] The TOMS, SBUV, SBUV-2, and OMI 340 nm reflectivity time series are able to provide estimates of UV cloud transmission C_T based on measured cloud and aerosol Lambert Equivalent Reflectivity R. Estimates for C_T have been improved by vector (polarization) radiative transfer solutions for plane parallel clouds of different optical thickness. The resulting cloud transmission factor C_T [*Krotkov et al.*, 2001] gives results that are close to a simple expression,

$$C_T = (1 - R)/(1 - R_G), \tag{3}$$

where R_G is the measured surface reflectivity and $R_G < R < 1$. This expression for C_T has been give by *Krotkov et al.* [2001] from energy conservation for nonozone absorbing wavelengths. C_T can also be derived from a Stokes calculation for a transmitting and reflecting surface over a reflecting ground [*Herman et al.*, 2009]. However, the presence of clear-sky absorbing aerosols or absorbing aerosol and cloud mixtures causes a significant reduction in R and C_T [*Krotkov et al.*, 2001], which are partly responsible for the observed differences between ground-based irradiance observations and those estimated from satellite data.

[23] When cloud reflectivity R is included in the Beer's law estimate of direct-beam irradiance, $F = Fo \exp(-\alpha\Omega \sec(\theta)) (1 - R)/(1 - R_G)$, then the differential form is

$$dF/F = -d\Omega/\Omega \; \alpha\Omega \sec(\theta) + dC_T/C_T. \tag{4}$$

[24] At short UV wavelengths, the diffuse flux becomes an important component of the total irradiance. For these wavelengths, the Beer's Law estimate of the irradiance reaching the ground should be $F = Fo \exp(-\alpha\Omega \sec(\theta)) (1 - R)/(1 - R_G) (1 + \Gamma)$, where Γ is the diffuse irradiance divided by the direct-beam irradiance. When the cloud or aerosol optical depths are comparable to or larger than the Rayleigh optical depth, then the term $d\Gamma/\Gamma$ should be added to equation (4). The situations where $d\Gamma$ cannot be neglected (e.g., within or below thick clouds or at large SZA) will be treated in a separate paper in terms of numerical radiative transfer solutions.

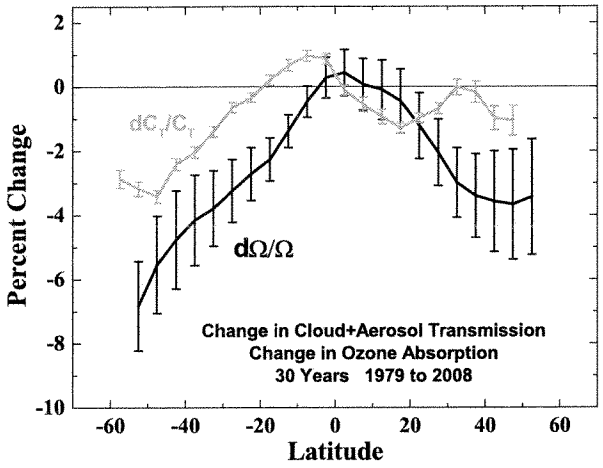

Figure 3. The 30 year percent change in zonal average annual ozone amount $d\Omega/\Omega$ and cloud plus aerosol transmission dC_T/C_T as a function of latitude. The error bars are estimated from the least squares fitting procedure.

[25] Equation (4) has proven to be accurate for estimating F_{UV} changes for small ozone changes (a few percent), while equation (1) can be used for large ozone amount changes. A comparison was run between numerical radiative transfer solutions RTS, including Rayleigh scattering, and equation (4) for a 1% change from three ozone values, 275, 375, and 475 DU for the wavelength range 290 to 350 nm and SZA = 30° [*Herman et al.*, 1999]. The largest difference between the RTS and equation (3) was 0.2% at 290 nm for 275DU and less than 0.1% for wavelengths larger than 310 nm.

[26] Equations (1), (2), and (4) can be used in a scattering atmosphere when the absorbing gas and changes in the absorbing gas are mainly in the stratosphere where there is little scattering. In this case, the scattered radiation received at the Earth's surface is proportional to the Beer's Law absorption of unscattered solar irradiance entering the lower troposphere. If the changes in the absorbing gas are mainly in the lower troposphere, where multiple scattering is important, then the Beer's Law formulation will underestimate the change in irradiance in proportion to the increased optical path caused by scattering. The Rayleigh optical depth at sea level [*Bodhaine et al.*, 1999] is about 1.06 at 310 nm, about 1.13 for 305 nm, and 1.2 for 300 nm, or about one third of the photons are scattered out of the forward beam and subject to small amount of additional absorption caused by a longer optical path through the troposphere. This means that the clear-sky underestimate of F_{UV} change caused by tropospheric ozone change and multiple scattering is small.

[27] *Fioletov and Evans* [1997] presented an extensive analysis of F_{UVB} and its dependence on total column ozone for clear and cloudy conditions. The analysis provides an empirical wavelength-by-wavelength measure of the increase of F_{UVB} for a 1% decrease of total ozone. The values for F_{UVB} change with ozone change were found to be essentially the same for clear and cloudy conditions (except for very heavy clouds) and are in good agreement with model results for longer wavelengths and moderate SZA.

[28] The Beer's Law method will miss some features of F_{UV} change, such as the momentary increase above clear-sky amounts caused by reflections from the sides of clouds and may not be accurate in mountain regions where the terrain reflectivity affects the irradiance differently than in relatively flat regions. Even in mountain regions, equations (1) or (2) will still represent the daily change in irradiance caused by changes in ozone amount. The Beer's Law method is not accurate over snow and ice, since the surface reflectivity is large and changing, and UV satellite data cannot detect the presence of clouds over ice/snow. It is also not accurate under thick clouds, where multiple scattering within the clouds produces additional wavelength-dependent absorption by ozone.

[29] For regions under thick clouds, the amount of F_{UVB} is small, so that the resulting error from neglecting multiple scattering within clouds will not affect long-term zonal average changes. For any changes in ozone amount, equation (1) can be used to estimate the changes in monochromatic irradiance and equation (2) for action spectrum weighted irradiance changes. If there are also changes in cloud reflectivity, then the dC_T/C_T term must be added as in equation (4).

[30] In order to estimate dF_{12}/F_2 from a time series of ozone amount and reflectivity, the solar zenith angle must be calculated as a function of local time t, latitude L, and seasonal declination angle δ. If the time of the day is taken as local noon, then the solar zenith angle θ is the latitude $L \pm \delta$ (the solar declination angle δ varying between ±23.45°) depending on the day of the year T (1 to 365) and the local time t (hours).

$$\cos(\theta) = \cos(L)\cos(\delta)\cos[\pi(t-12)/12] + \sin(L)\sin(\delta), \quad (5)$$

where δ can be obtained from ephemeris data or from approximations of varying accuracy. The simplest approximation, equation (6), is given by assuming that the Earth's orbit is a circle, where the argument of the cosine is in degrees,

$$\delta = -23.45\ \cos[0.986(T+10)]. \quad (6)$$

[31] Reflectivity data are taken from the arithmetically averaged merged data set described by *Herman et al.* [2009], but based only on N7-TOMS, and the SBUV-2 series (also see Figure 2). Before dR can be used in equation (2), the function dR/R must be transformed into cloud transmission change dC_T/C_T using equation (3). Based on satellite data, the 30 year percent change in ozone and C_T are shown in Figure 3. The cloud plus aerosol transmission data suggest that there has been dimming in the SH, and a smaller long-term hemispherical dimming in the NH. Similarly, the percent change in ozone amount has been larger in the SH than in the NH.

5. Short-Term Factors Affecting Irradiance

[32] UV radiation reaching the Earth's surface varies on all time scales, from seconds to seasons to years, and varies strongly with latitude (solar zenith angle for UVA and UVB, and with ozone amount for UVB). The cloud plus aerosol transmission modulated latitude dependence of UV irradiance is clearly shown in global maps [*Herman et al.*, 1999].

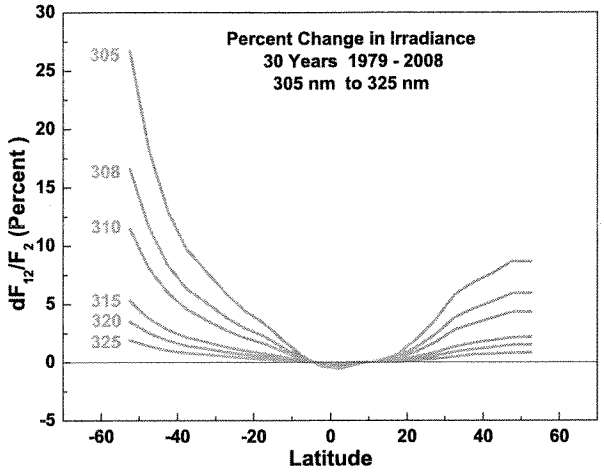

Figure 4. Percent annual changes in zonal average 305 to 325 nm and erythemal irradiances from changes in ozone amount for 30 years (1979 to 2008) calculated from equation (1). For $\lambda > 325$ nm, the change is negligible.

Day-to-day ozone-caused changes in UVB irradiance can be significant, but are usually smaller than changes due to cloud cover, because the stratospheric abundance of ozone usually changes as a moderate percentage (e.g., ±15% at midlatitudes) of its seasonally changing mean value. Broad seasonally repeating cloud patterns also cause changes on daily and monthly time scales as the weather changes. Minor geographical shifts in these cloud patterns have major effects on ground-based trend estimates of UV irradiance, while having only a small effect on zonal or regional average irradiances.

[33] On longer time scales (decadal), most regional changes in cloud plus aerosol reflectivity have been small [*Herman et al.*, 2009], so that global and zonal average changes in F_{UVB} due to long-term ozone depletion are dominant over long-term cloud-change effects, except in the equatorial zone where the long-term ozone changes are not statistically significant. In some regions (e.g., northern Europe), decadal-term cloud and aerosol changes are also important. F_{UVA} changes for wavelengths longer than 340 nm are controlled by all of the above factors except ozone. Local midlatitude UV irradiance reductions caused by clouds frequently range up to 50%, and occasionally to nearly 100%, which is larger than the day-to-day local 305 nm UV variability caused by ozone (25%), and comparable to changes at 300 nm caused by ozone (since $RAF_{300} > RAF_{305}$).

[34] Daily ozone data from Nimbus-7/TOMS, obtained during June within the entire 5° latitudinal zone centered at 40°N, shows that the ozone amount can vary by 50 DU about the mean value of 350 DU, or $d\Omega/\Omega = \pm 0.14$. The day-to-day June ozone variation is obtained from figures similar to those shown by *Herman et al.* [1995]. Using an average noon SZA for late June of about 23° and an ozone absorption coefficient for 305 nm $\alpha = 4.75$ cm^{-1} yields a typical 305 nm irradiance change $dF/F = -d\Omega/\Omega$ $\alpha\Omega$ sec(θ) = ±0.14 * 4.75 * 0.35 * 1.09 = ±0.25. That is, for clear-sky conditions, the 305 nm irradiance typically changes by ±25% during late June just from to day-to-day ozone changes. As will be discussed later, the day-to-day variability of clear-sky 40°N UV June irradiance is much larger than the irradiance increase caused by long-term June decrease in ozone from 1979 to 2008. These variations are the basis for supplying daily UV index information along with the weather report.

[35] Other factors, such as Rayleigh scattering and land/ocean surface reflectivity, affect the magnitude of measured or theoretically estimated UV irradiance. However, these factors (except for snow and ice) do not significantly affect the short- or long-term variations in irradiance, since their changes are small. Hourly or daily changes in Rayleigh scattering follow the small fluctuations in atmospheric pressure, which usually are less than 2%. There have been no long-term changes in mean atmospheric pressure. The UV surface reflectivity R_G is small (3 RU to 10 RU) and almost constant with time except in regions seasonally or permanently covered with snow or ice. Based on radiative transfer studies [*Herman et al.*, 1999; *Pucai and Lenoble*, 1996; *Lenoble*, 1998], clear-sky atmospheric backscattering to the surface contributes less than 0.4 R_G to the measured UV irradiance, which is quite small for most ice-/snow-free scenes. The maximum atmospheric backscattering occurs near 320 nm because of the combined effects of Rayleigh scattering and ozone absorption. In the polar regions, or in areas with snow/ice cover, the backscattered irradiance can be a significant fraction of the downwelling irradiance [*Lenoble*, 1998].

[36] The local amount of F_{UV} reaching the earth's surface is affected by air pollution, i.e., scattering and absorption by aerosols (black and organic carbon, hydrocarbons, dust, and smoke), absorption by tropospheric O_3, NO_2, and other gases. These can cause typical reductions in F_{UV} up to 15% in polluted sites, but with much higher reductions (e.g., more than 25%) occurring in certain highly polluted cities, for example, occasionally in Los Angeles and frequently in Beijing. A recent study has quantified similar effects in Tokyo, showing that tropospheric extinctions were up to 40% larger than in the clean atmosphere of New Zealand [*McKenzie et al.*, 2008] and that F_{UVA} could occasionally be strongly affected by high levels of tropospheric NO_2. Since aerosols of most types affect UV and visible radiation at all wavelengths, pollution abatement, especially in highly polluted regions, can decrease the atmospheric reflectivity and absorption, which has the effect of increasing the amount of UV radiation reaching the ground. Short-term reductions in surface F_{UV} can be much higher in regions affected by smoke from biomass burning, or by major dust storms that frequently occur in Africa and parts of China.

6. Estimating Zonal Average Monochromatic UV Change

[37] The estimated annual changes in irradiances caused by ozone changes (Figures 1 and 3 and equation (1)) are given for six wavelengths (Figure 4). The wavelength range from 305 to 325 nm includes the region where the DNA damage, vitamin D, and erythemal action spectra have their maximum effect.

[38] For middle and high latitudes, the F_{UV} changes that occur between the spring and autumn equinoxes are of more

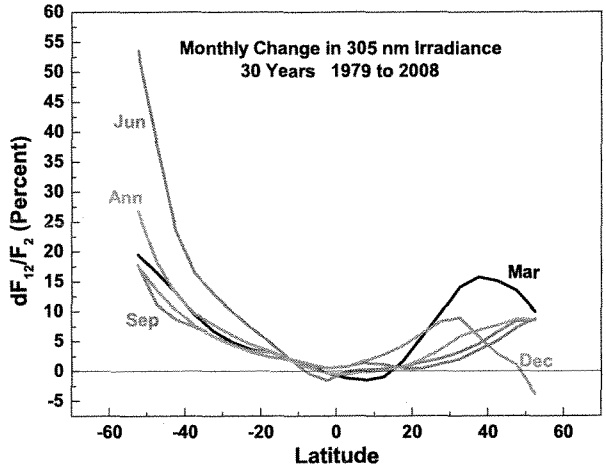

Figure 5. Monthly and annual (Ann) percent changes in zonal average 305 nm irradiance from changes in ozone amount for 30 years (1979 to 2008) calculated from equation (1).

concern than those that occur during the winter months, since the sun is most intense during the summer months (minimum SZA) and least intense during the winter months (maximum SZA). In the NH, the changes in ozone amount and F_{UVB} that have occurred during the spring months (see March in Figure 5) dominate those that have occurred during any other season.

[39] As can be seen in Figures 4, 5, and 6, the changes in the SH summer irradiance caused by changes in O_3 were much larger than the corresponding NH summer changes. The same is true during the winter months, following a larger general decline in ozone amount (increase in irradiance) in the SH compared to the NH (Figure 3). The large changes in F_{UVB} that have occurred in the SH summer and autumn months (December to March, Figure 5) are of concern, since these are the months when it is most likely that there will be human exposure to UVB not protected by clothing, as well as material and plant damage. Figures 5 and 6 show large increases at high SH latitudes during winter months (May and June). However, the large winter increases correspond to months when the absolute amount of zonal average UV is usually small.

7. Action Spectra and Irradiance Changes

[40] An action spectrum $A(\lambda)$ is an irradiance weighting function of wavelength λ that estimates the relative strength of a process (e.g., biological process or material degradation) for each wavelength in a range from λ_1 to λ_2. The action spectrum is multiplied by the irradiance $F(\lambda,t)$ to obtain a production or effect function P(t). A direct correlation of weighted dose amounts for any causal effect is not given by $A(\lambda)$, but just indicates the relative effect of each wavelength.

[41] Typical action spectra have been estimated for skin reddening for Caucasian males, plant growth, vitamin D production, nonmelanoma cancer production, DNA damage, etc. The CIE vitamin D action spectrum $A_{Vit\text{-}D}$ [*Bouillon et al.*, 2006] is based on the original paper by *MacLaughlin et al.* [1982]. The vitamin D production was obtained in the laboratory from a limited sample of "surgically separated skin." An accurate functional fit to the logarithm of the data (Figure 7a) is given ($270 < \lambda < 330$ nm) in Table 2 along with graphs (Figures 7b, 7c, 7d) for the logarithm of three other common action spectra, DNA damage A_{DNA}, plant growth A_{PLA}, and erythemal A_{ERY}.

[42] Previous studies have proposed fitting functions for DNA damage and plant growth response action spectra [e.g., *Bernhard et al.*, 1997; *Green et al.*, 1974; *Bouillon et al.*, 2006].

[43] In order to calculate the change in action spectrum weighted irradiance as a function of θ = SZA and ozone amount, the summation over wavelength λ must be obtained, $P = S\, A(\lambda)\, F(\lambda)\, \Delta\lambda$, and the ratio P_1/P_2 calculated for a range of ozone values $\Omega_1 < \Omega < \Omega_2$. If the standard empirical form $P_1/P_2 = (\Omega_2/\Omega_1)^{RAF}$ is assumed [*Madronich*, 1994], then $RAF(\theta, \Omega)$ can be derived from

$$RAF(\theta, \Omega_1/\Omega_2) = Ln(P_1/P_2)/Ln(\Omega_2/\Omega_1). \quad (7)$$

[44] The results from this calculation have been shown for erythemal action spectrum $A_{ERY}(\lambda)$ and instrumental response functions that approximate $A_{ERY}(\lambda)$ [*Seckmeyer et al.*, 2005] for the ozone amount range 100 DU $< \Omega <$ 600 DU. When computed from equations (2) and (7), the results for $RAF(\theta,\Omega/600)$ are as shown in Figure 8 for $A_{ERY}(\lambda)$, and are similar to those obtained by *Seckmeyer et al.* [2005] using numerical solutions of vector or scalar radiative transfer calculations.

[45] If the range of ozone is limited to 200 DU $< \Omega <$ 600 DU, then the results for $RAF(\theta)$ and the coefficient $U(\theta)$ are independent of Ω and can be fitted by the functional form shown in equation (8). The independence from Ω is more convenient for analyzing irradiance data than the double-valued $RAF(\theta, \Omega)$ results shown in Figure 8.

$$P_1/P_2 = U(\theta)(\Omega_2/\Omega_1)^{RAF(\theta)} \quad \text{or}$$
$$dP_{12}/P_2 = U(\theta)(d\Omega_{12}/\Omega_2 + 1)^{-RAF(\theta)} - 1. \quad (8)$$

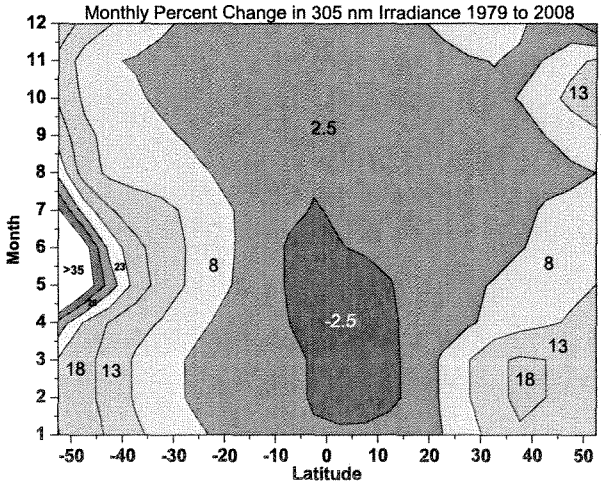

Figure 6. Seasonal percent change in 305 nm UV irradiance after 30 years, 1979–2008, calculated from equation (1).

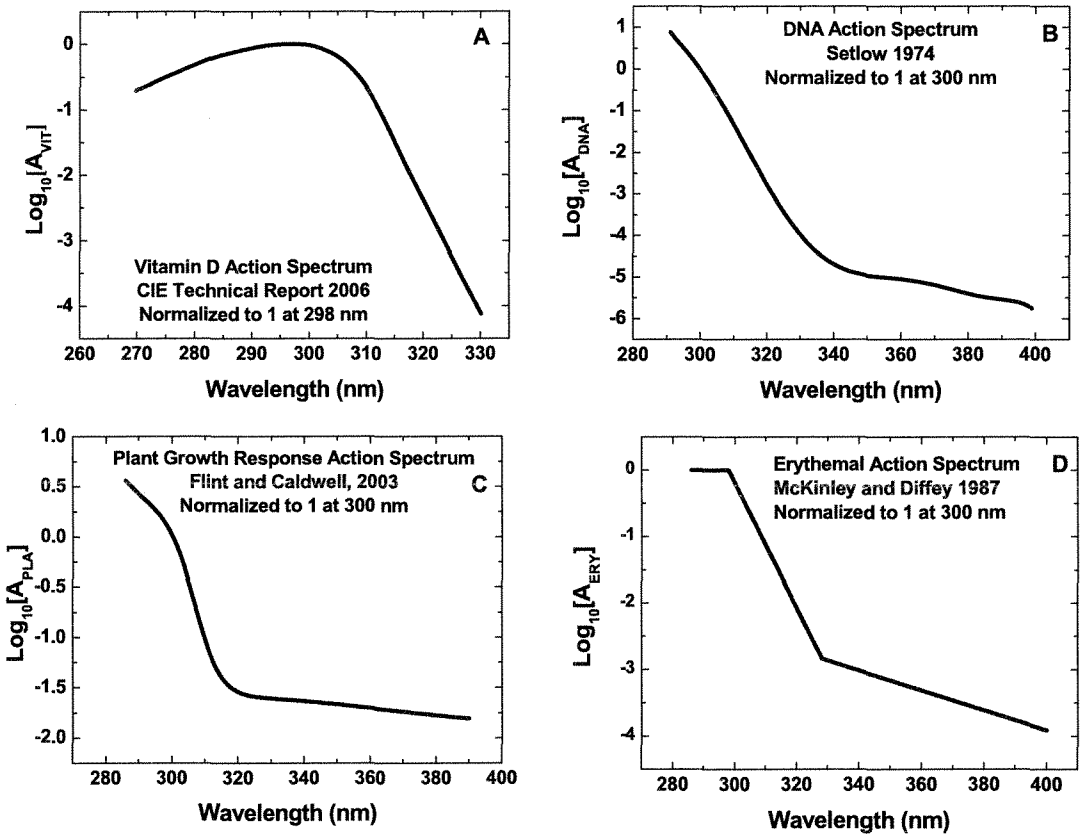

Figure 7. (a) Fit to vitamin D action spectrum [*Bouillon et al.*, 2006] $270 < \lambda < 330$ nm. (b) Fit to DNA damage action spectrum [*Setlow*, 1974] $290 < \lambda < 400$ nm. (c) Fit to plant growth response action spectrum [*Flint and Caldwell*, 2003] $285 < \lambda < 390$ nm. (d) Fit to erythemal action spectrum [*McKinley and Diffey*, 1987] $250 < \lambda < 400$ nm.

Table 2. Function Fit to Four UV Action Spectra of Figure 6

Spectrum	Function	Coefficients
Fit to vitamin-D spectrum [*Bouillon et al.*, 2006] $A_{Vit\text{-}D}$	$Log_{10}(A_{Vit\text{-}D}) = \frac{A+C\lambda^{0.5}+E\lambda+G\lambda^{1.5}}{1.0+B\lambda^{0.5}+D\lambda+F\lambda^{1.5}}$ $250 < \lambda < 314$ nm	A = −2.765061017624136 B = −0.1118147807085076 C = 0.3214640452394133 D = 0.003131276674508003 E = −0.009342852420667167 F = 0.0 G = 0.0
Fit to DNA damage spectrum [*Setlow*, 1974] A_{DNA}	$Log_{10}(A_{DNA}) = \frac{A+C\lambda^{0.5}+E\lambda+G\lambda^{1.5}}{1.0+B\lambda^{0.5}+D\lambda+F\lambda^{1.5}}$ $290 < \lambda < 400$ nm	A = −0.1090717334891702 B = −0.1578036701734071 C = 0.01546956801974633 D = 0.008268275171175154 E = −0.0005294176165721459 F = −0.0001436582640327567 G = 0.0
Fit to plant growth response action spectrum [*Flint and Caldwell*, 2003] A_{PLA}	$Log_{10}(A_{PLA}) = \frac{A+C\lambda^{0.5}+E\lambda+G\lambda^{1.5}}{1.0+B\lambda^{0.5}+D\lambda+F\lambda^{1.5}}$ $285 < \lambda < 390$ nm	A = −2.747265993518105 B = −0.1791860260727771 C = 0.4772684658484249 D = 0.01068302156756403 E = −0.02764643975624155 F = −0.0002119599411078172 G = 0.0005339842703179307
Fit to erythemal action spectrum [*McKinley and Diffey*, 1987] A_{ERY}	$Log_{10}(A_{ERY})$ $250 < \lambda < 400$ nm $250 < \lambda < 298$ nm $298 < \lambda < 328$ nm $328 < \lambda < 400$ nm	$Log_{10}(A_{ERY}) = 0$ $Log_{10}(A_{ERY}) = 0.094(298 - \lambda)$ $Log_{10}(A_{ERY}) = 0.015(139 - \lambda)$

[46] Theoretically calculated RAF(θ) and U(θ) values for the four action spectra in Figure 7 are given in Figures 9a and 9b, and the fitting functions for each in Tables 3 and 4. All four spectra have U(θ) values near 1, especially U_{ERY} and U_{PLA}. For relatively narrow A(λ) spectra, mostly contained in the UVB region, the behavior of the action spectra RAF(θ) is similar to single wavelength RAFs, namely increasing RAF with SZA. More broadly based

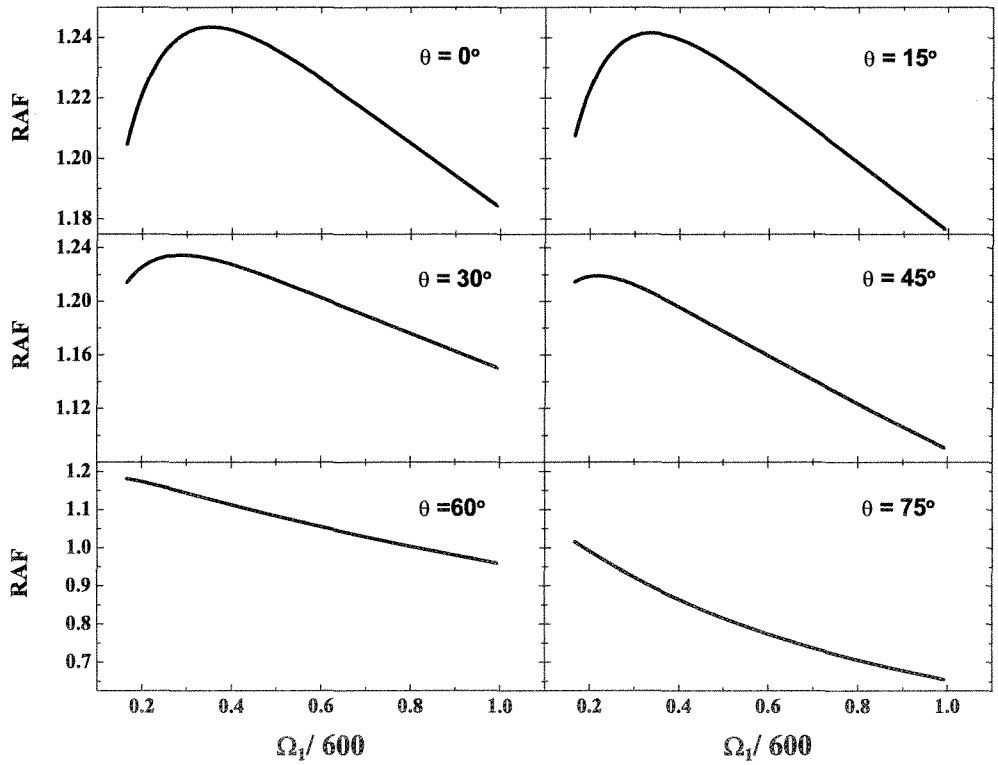

Figure 8. RAF(θ, Ω/600) for 100 DU < Ω < 600 DU and 0° < θ < 75° for $A_{ERY}(\lambda)$.

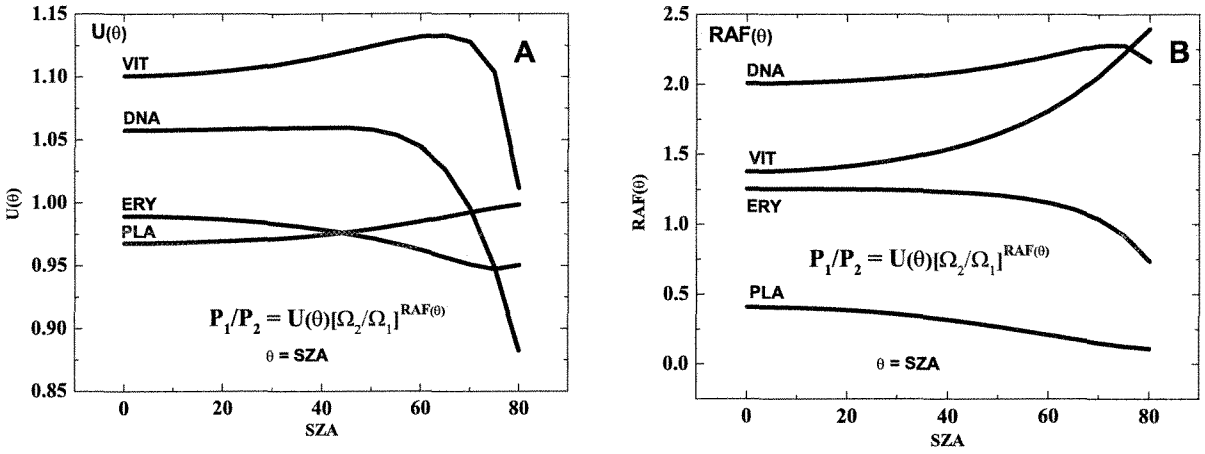

Figure 9. The variation of (a) U(θ) and (b) RAF(θ) for the four spectra in Figure 7.

spectra have RAF(θ) values that are nearly constant for $\theta < 40°$, and decrease for larger values. Very wide action spectra, such as the plant growth spectrum, cause RAF(θ) to decrease for all $\theta > 0$.

[47] The RAF(θ) can be derived from spectrally resolved experimental irradiance data for each action spectrum or from an appropriate broadband instrument. This has been done for the erythemal irradiance F_{ERY} using measurements from Mauna Loa, Hawaii [*Bodhaine et al.*, 1997]. The resulting measured variation of RAF with θ is shown in Figure 10 along with a theoretical calculation based on equation (8) applied to erythemal weighting A_{ERY}. This shows that the power law behavior $F_1/F_2 = U(\theta)\ (\Omega_2/\Omega_1)^{RAF(\theta)}$, derived from the physically based Beer's Law (equation (1)) for absorption in the atmosphere, agrees with measurements within the stated experimental error bars. The cause for the increase (e.g., 1.25 to 1.4 at $\theta = 55°$) in measured RAF(θ) relative to calculated RAF(θ) for $35° < \theta < 65°$ was considered as statistically not significant, as indicated by the error bars, [*Bodhaine et al.*, 1997] due to an insufficient number of measurements. The behavior of RAF(θ) is as expected from a mix of UVB and UVA wavelengths, as the importance of UVB decreases with increasing θ. For the erythemal irradiance $0.95 < U(\theta) < 0.98$ so that the variation of U(θ) can be neglected as a good approximation (i.e., $U(\theta) \sim 1$).

[48] Measurements of erythemal irradiance were made at the South Pole from 1 February 1991 to 12 December 1992 [*Booth and Madronich*, 1994], which they estimated could be fit with a power law of RAF = 1.1, which is equivalent to having an average SZA of 68° based on Figure 10 (see small circle).

[49] The 30 year percent change in zonal average DNA damage, erythemal, vitamin D, and plant growth weighted irradiances as a function of latitude (Figure 11) can be estimated from the monthly and zonal averaged ozone time series by using equation (8) and Tables 3 and 4. Also shown for comparison are the percent changes (using equation (1)) in six monochromatic irradiances (305, 308, 310, 315, 320, and 325 nm) from Figure 3, which show different behavior compared to the action spectrum weighted irradiances. The estimations are restricted to latitudes between 53°S to 53°N because the estimation of the RAF was for SZA < 80°. During the winter solstice at 53° latitude, the noon SZA is 76°. The estimation of RAFs for large SZA > 80° should be done with a spherical geometry corrected radiative transfer analysis. This is because the direct irradiance from the sun becomes small as the SZA increases, causing the scattered component to become more important. The result is that the RAF is no longer a cosine function of SZA.

[50] The basic shapes of the action spectrum weighted irradiance changes shown in Figure 11 follow the ozone changes with latitude, with the DNA damage weighted irradiances showing the largest changes. The plant growth weighted irradiances show the least increase with decreasing ozone since it is heavily weighted in the UVA range. The erythemal and vitamin D irradiance changes are very similar with latitude, except when the ozone change is large as in the Southern Hemisphere.

[51] When cloud plus scattering aerosol changes are included in the estimate of irradiance changes based on equation (3), the average net change $\Delta P/P$ in the SH is decreased, and is increased in the NH (Figure 12), since

Table 3. Fit to Four Radiation Amplification Factors of Figure 8[a]

	$RAF(\theta) = (A + C\,\theta^2 + E\,\theta^4)/(1 + B\,\theta^2 + D\,\theta^4)\ 200 < \Omega < 600$ DU			
	RAF_{ERY}	RAF_{DNA}	RAF_{PLA}	RAF_{VIT}
A	1.252946426768929	2.006603342348651	0.4073379778930943	1.376475606090887
B	−0.0001303044739461282	−0.000222243468041799	−9.687026334483537D-05	−0.000214638508166775
C	−0.000168798247039009	−0.0000400537916876323	−9.459907795864133D-05	−0.0002075927499557957
D	3.042379353697366D-09	1.23788082612675D-08	5.797211763472776D-09	1.07674832236824D-08
E	9.980359359513303D-10	1.861486615239331D-08	6.477474389629154D-09	2.773081357827353D-09

[a]Read, for example, D-09 as $\times 10^{-9}$; RAF, radiation amplification factor.

Table 4. Fit to Four U(θ) Coefficients of Figure 8[a]

	$U(\theta) = (A + C\,\theta^2 + E\,\theta^4)/(1 + B\,\theta^2 + D\,\theta^4)$ $200 < \Omega < 600$ DU			
	U_{ERY}	U_{DNA}	U_{PLA}	U_{VIT}
A	0.9893166937523816	1.057388605406105	0.9677509633289078	1.100670506751948
B	−0.0001958712159405352	−0.0002569199889246916	−0.0001466532279117854	−0.0002018558752315443
C	−0.0002000146908946258	−0.0002690240644531278	−0.0001385678657904003	−0.0002128877079207862
D	8.648859003644555E-09	1.947048385487091D-08	1.300241240363876D-08	9.207189814175676D-09
E	9.434858625854004E-09	1.952293904580326D-08	1.250439205414737D-08	8.497322891667962D-09

[a]Read, for example, D-09 as $\times 10^{-9}$.

cloud transmission C_T has decreased in the SH and has increased in the NH (Figure 3).

[52] The average changes in erythemal weighted irradiance are modest at higher latitudes in both hemispheres, 3.1% at 50°N, near the Canadian border and 5.2% at 50°S latitude near the southern tip of South America. However, in the SH, the net increase, $\Delta P/P$, is less than the clear-sky increase, dP_{12}/P_2, since there is a partial offset by an average decrease in cloud transmission. For clear-sky days, the increase in erythemal irradiance dP_{12}/P_2 at 50°S is about 8.5%, a change that is considerably larger and potentially more dangerous than the average value for clear and cloudy days (solid line). Further north at the latitude of Buenos Aires (34.6°S), the clear-sky increase is about 5.6%. In the NH the increase is only 4.4% at the latitude of Washington, DC (38.9°N). The zonal average irradiance increases, obtained using combined cloud plus aerosol transmission and ozone absorption, will vary locally and regionally because of different amounts of local cloud and aerosol cover.

[53] As shown in Figure 12, the 30 year percent change in irradiance is mostly caused by changes in ozone amount except near the equator where the ozone changes are not significant. The apparent leveling off with latitude of ozone change $d\Omega_{12}/\Omega_2$ between 35°N and 50°N also appears in the expression for monochromatic dF_{12}/F_2, but to a lesser degree because of the increase of sec(θ) with latitude. The increase in cloud plus aerosol reflectivity (decrease in C_T) at high southern latitudes moderates the average irradiance increase caused by ozone decreases. However, on clear-sky days the increase in irradiance is mostly governed by ozone change plus a very small change from possible changes in aerosol amounts.

[54] Figure 13 shows the monthly percent change in dP_{12}/P_2 for four action spectra weighted irradiances $P_{ACT} = P_{ERY}$(Month, Lat), P_{DNA}(Month, Lat), P_{PLA}(Month, Lat), and P_{VIT}(Month, Lat) from 1979 to 2008. P_{ERY}, which is associated with sunburn and the incidence of skin cancer, has increased dramatically in the SH and moderately in the NH. In the SH spring (October and November) the increases in P_{ERY} are similar to the NH spring (April and May) changes of about 5% to 7% at 40° to 45° latitude. However, the SH summer changes in December to February are much larger than in the NH (June to August) where the changes range from 5% in June to 3% for July and August. The major population centers in middle and southern South America, Southern Africa, Australia, and New Zealand have significant increases in P_{ERY}. The increases in P_{ERY} have occurred during most of the spring and summer when the solar UV irradiance exposure is at a maximum (more clear

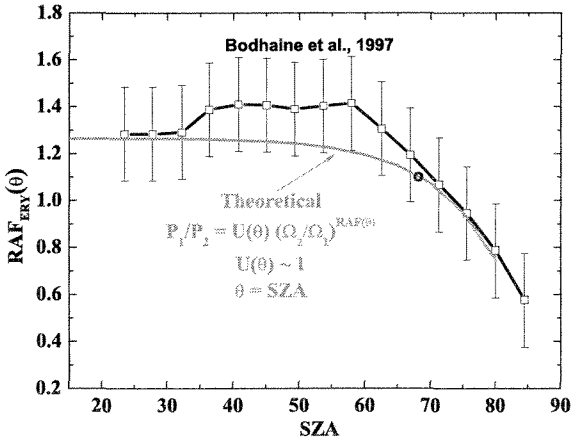

Figure 10. RAF_{ERY} variation with θ (SZA) for the erythemal action spectrum from data obtained at Mauna Loa Hawaii [*Bodhaine et al.*, 1997] compared with a theoretical calculation based on equations (2) and (6) and Tables 3 and 4. The small circle is located at $\theta = 68°$ with a RAF value of 1.1.

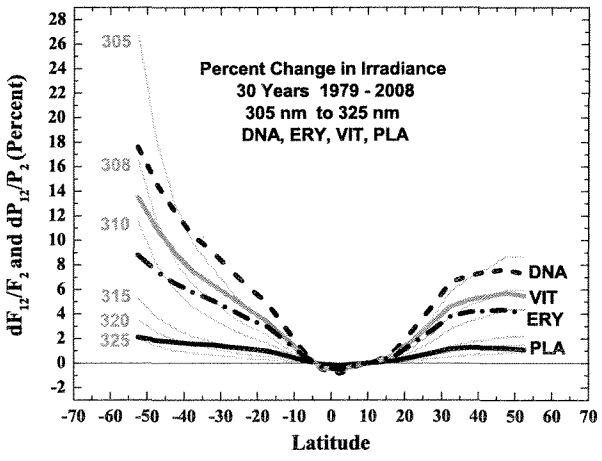

Figure 11. Percent changes dP_{12}/P_2 in DNA damage (DNA), erythemal (ERY), vitamin D (VIT), and plant growth (PLA) action spectra weighted irradiances from total change in ozone amount for 30 years (1979 to 2008). Also shown for comparison are six monochromatic dF_{12}/F_2 irradiance changes from Figure 3. The action spectra calculations are based on Tables 3 and 4 and equation (8).

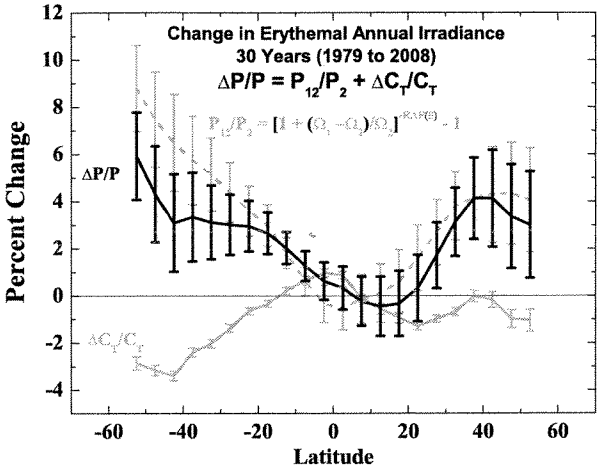

Figure 12. The change in erythemal irradiance ($\Delta P/P$, black solid line) caused by changes in reflectivity and cloud transmission ($\Delta C_T/C_T$, gray solid line) and the changes in ozone amount Ω (dP_{12}/P_2, dashed line). The dP_{12}/P_2 represents the clear-sky changes in erythemal irradiance. Error bars are estimated from the linear least squares fitting procedure.

days as well as seasonally declining ozone going into the summer).

[55] To the extent they are sensitive to changes in ozone amount, the three other monthly changes in P_{ACT} behave in a similar manner to P_{ERY}, with the largest changes occurring for P_{DNA}. Since the UV index is based on a multiplicative scaling of erythemal irradiance, the percent change in UV index is the same as the change in P_{ERY}.

8. Summary

[56] Satellite measurements of ozone and cloud plus aerosol reflectivity have been used to estimate zonal average changes in UV irradiance (300 to 325 nm) over the past 30 years (1979 to 2008) using a simplified radiative transfer approach based on Beer's Law for both monochromatic and action spectrum weighted irradiances. Integrating Beer's Law attenuation of UV irradiance over the wavelength spectrum of an action spectrum yields the RAF inverse power law relation of irradiance change to ozone change. The ozone-based trend estimates may not apply to local urban or industrial regions where absorbing aerosols may have long-term changes (e.g., Beijing or Los Angeles). The largest zonal average increases in UV irradiance occurred in

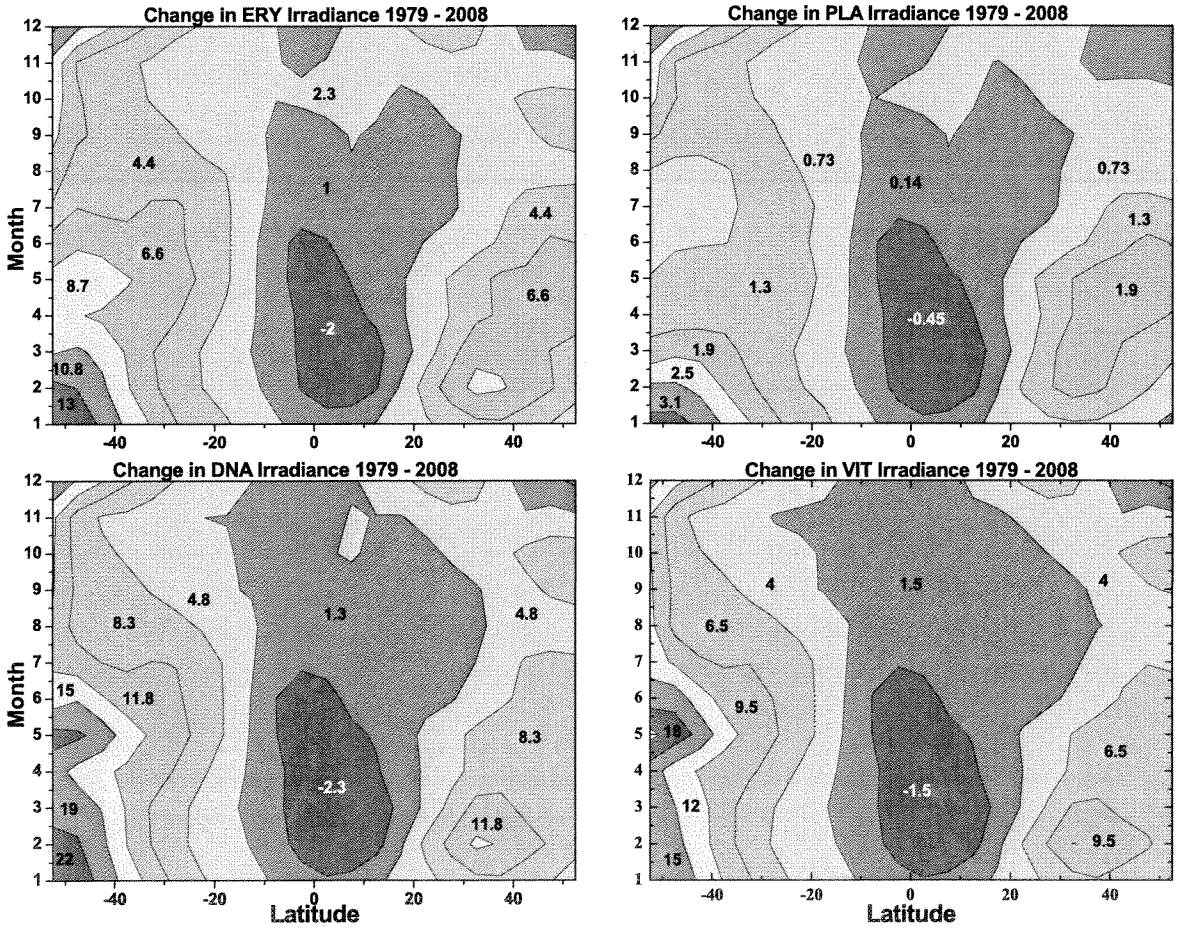

Figure 13. Percent change in four action spectra weighted irradiances P_{ACT} for the period 1979 to 2008 as a function of latitude and month. The calculations are based on equation (6) and Tables 3 and 4.

the Southern Hemisphere where the ozone decrease has been the largest. For clear-sky conditions at 50°S the following ozone caused irradiance zonal average changes are estimated (305 nm, 23%; erythemal, 8.5%; 310 nm, 10%; vitamin D production, 12%). These are larger than at 50°N (305 nm, 9%; erythemal, 4%; 310 nm, 4%; vitamin D production, 6%). At the latitude of Buenos Ares, Argentina (34.6°S) the clear-sky irradiance increases are comparable to the increases near Washington, D. C. (38.9°N): 305 nm, 9% and 7%; erythemal, 6% and 4%; vitamin D production, 7% and 5%, respectively. The larger changes that occurred at higher latitudes in the Southern Hemisphere were only partially moderated by a strongly latitude-dependent apparent increase in cloud and aerosol reflectivity leading to reduced cloud plus aerosol transmission to the earth's surface. This differs from the Northern Hemisphere, where midlatitude and high-latitude cloud plus aerosol reflectivity caused negligible decreases in annual average transmission.

[57] **Acknowledgments.** The author would like to thank the satellite ozone processing group and MEASURES reflectivity team at Goddard Space Flight Center and SSAI for the production of the ozone and reflectivity time series.

References

Bener, P. (1972), Approximate values of intensity of natural ultraviolet radiation for different amounts of atmospheric ozone, *Tech. Rep. AD-752-115*, Natl. Tech. Inf. Serv., Springfield, Va.

Bernhard, G., B. Mayer, G. Seckmeyer, and A. Moise (1997), Measurements of spectral solar UV irradiance in tropical-Australia, *J. Geophys. Res.*, *102*(D7), 8719–8730, doi:10.1029/97JD00072.

Blumthaler, M., M. Salzgeber, and W. Ambach (1995), Ozone and ultraviolet-B irradiances: Experimental determination of the radiation amplification factor, *Photochem. Photobiol.*, *61*, 159–162, doi:10.1111/j.1751-1097.1995.tb03954.x.

Bodhaine, B. A., E. G. Dutton, D. J. Hofmann, R. L. McKenzie, and P. V. Johnston (1997), UV measurements at Mauna Loa: July 1995 to July 1996, *J. Geophys. Res.*, *102*(D15), 19,265–19,273, doi:10.1029/97JD01391.

Bodhaine, B. A., N. B. Wood, E. G. Dutton, and J. R. Slusser (1999), On Rayleigh optical depth calculations, *J. Atmos. Oceanic Technol.*, *16*, 1854–1861, doi:10.1175/1520-0426(1999)016<1854:ORODC>2.0.CO;2.

Booth, C. R., and S. Madronich (1994), Radiation amplification factors: Improved formulation accounts for large increases in ultraviolet radiation associated with Antarctic ozone depletion, in *Ultraviolet Radiation in Antarctica: Measurement and Biological Effects*, *Antarct. Res. Ser.*, vol. 62, edited by C. S. Weiler and P. S. Penhale, pp. 39–52, AGU, Washington, D. C.

Bouillon, R., J. Eisman, M. Garabedian, M. Holick, J. Kleinschmidt, T. Suda, I. Terenetskaya, and A. Webb (2006), Action spectrum for the production of previtamin D3 in human skin, *CIE 174-2006*, Int. Comm. on Illumination, Vienna.

Fioletov, V. E., and W. F. J. Evans (1997), The influence of ozone and other factors on surface radiation, in *Ozone Science: A Canadian Perspective on the Changing Ozone Layer*, edited by D. I. Wardle et al., pp. 73–79, Univ. of Toronto Press, Toronto, Ont., Canada.

Fioletov, V. E., L. J. B. McArthur, J. B. Kerr, and D. I. Wardle (2001), Long-term variations of UV-B irradiance over Canada estimated from Brewer observations and derived from ozone and pyranometer measurements, *J. Geophys. Res.*, *106*(D19), 23,009–23,028, doi:10.1029/2001JD000367.

Fioletov, V. E., G. E. Bodeker, A. J. Miller, R. D. McPeters, and R. Stolarski (2002), Global and zonal total ozone variations estimated from ground-based and satellite measurements: 1964–2000, *J. Geophys. Res.*, *107*(D22), 4647, doi:10.1029/2001JD001350.

Fioletov, V. E., M. G. Kimlin, N. Krotkov, L. J. B. McArthur, J. B. Kerr, D. I. Wardle, J. R. Herman, R. Meltzer, T. W. Mathews, and J. Kaurola (2004), UV index climatology over North America from ground-based and satellite estimates, *J. Geophys. Res.*, *109*, D22308, doi:10.1029/2004JD004820.

Flint, S. D., and M. M. Caldwell (2003), A biological spectral weighting function for ozone depletion research with higher plants, *Physiol. Plant.*, *117*, 137–144.

Gleason, J. F., et al. (1993), Record low global ozone in 1992, *Science*, *260*, 523–526, doi:10.1126/science.260.5107.523.

Green, A. E. S., T. Sawada, and E. P. Shettle (1974), The middle ultraviolet reaching the ground, *Photochem. Photobiol.*, *19*, 251–259, doi:10.1111/j.1751-1097.1974.tb06508.x.

Herman, J. R., et al. (1995), Meteor-3/Total Ozone Mapping Spectrometer observations of the 1993 ozone hole, *J. Geophys. Res.*, *100*(D2), 2973–2983, doi:10.1029/94JD02316.

Herman, J. R., P. K. Bhartia, J. Ziemke, Z. Ahmad, and D. Larko (1996), UV-B radiation increases (1979–1992) from decreases in total ozone, *Geophys. Res. Lett.*, *23*, 2117–2120, doi:10.1029/96GL01958.

Herman, J. R., N. A. Krotkov, E. A. Celarier, D. Larko, and G. Labow (1999), The distribution of UV radiation at the Earth's surface from TOMS measured UV-backscattered radiances, *J. Geophys. Res.*, *104*(D10), 12,059–12,076, doi:10.1029/1999JD900062.

Herman, J. R., G. Labow, N. C. Hsu, and D. Larko (2009), Changes in cloud cover derived from reflectivity time series using SeaWiFS, N7-TOMS, EP-TOMS, SBUV-2, and OMI radiance data, *J. Geophys. Res.*, *114*, D01201, doi:10.1029/2007JD009508.

Kalliskota, S. J., J. Kaurola, P. Taalas, J. R. Herman, E. Celarier, and N. Krotkov (2000), Comparison of daily UV doses estimated from Nimbus-7/TOMS measurements and ground-based spectroradiometric data, *J. Geophys. Res.*, *105*(D4), 5059–5067, doi:10.1029/1999JD900926.

Krotkov, N. A., P. K. Bhartia, J. R. Herman, V. Fioletov, and J. Kerr (1998), Satellite estimation of spectral surface UV irradiance in the presence of tropospheric aerosols: 1. Cloud-free case, *J. Geophys. Res.*, *103*(D8), 8779–8879, doi:10.1029/98JD00233.

Krotkov, N. A., J. R. Herman, P. K. Bhartia, Z. Ahmad, and V. Fioletov (2001), Satellite estimation of spectral surface UV irradiance: 2. Effect of horizontally homogeneous clouds, *J. Geophys. Res.*, *106*(D11), 11,743–11,759.

Latarjet, R. (1935), Influences des variations l'ozone atmospherique sur l'activite biologique du rayonnment solaire, *Rev. Opt. Theor. Instrum.*, *14*, 398–414.

Lenoble, J. (1998), Modeling of the influence of snow reflectance on ultraviolet irradiance for cloudless sky, *Appl. Opt.*, *37*, 2441–2447, doi:10.1364/AO.37.002441.

Levelt, P. F., G. H. J. van den Oord, M. R. Dobber, A. Malkki, H. Visser, J. de Vries, P. Stammes, J. O. V. Lundell, and H. Saari (2006), The ozone monitoring instrument, *IEEE Trans. Geosci. Remote Sens.*, *44*(5), 1093–1101, doi:10.1109/TGRS.2006.872333.

Liley, J. B. (2009), New Zealand dimming and brightening, *J. Geophys. Res.*, *114*, D00D10, doi:10.1029/2008JD011401.

MacLaughlin, J. A., R. R. Anderson, and M. F. Holick (1982), Spectral character of sunlight modulates photosynthesis of previtamin D3 and its photoisomers in human skin, *Science*, *216*, 1001–1003, doi:10.1126/science.6281884.

Madronich, S. (1993), The atmosphere and UV-B radiation at ground level, in *Environmental UV Photobiology*, edited by L. O. Björn and A. R. Young, pp. 1–39, Plenum, New York.

Madronich, S. (1994), Increases in biologically damaging UV-B radiation due to stratospheric ozone reductions: A brief review, *Arch. Hydrobiol.*, *43*, 17–30.

McKenzie, R. L., G. Seckmeyer, A. F. Bais, J. B. Kerr, and S. Madronich (2001), Satellite retrievals of erythemal UV dose compared with ground-based measurements at northern and southern midlatitudes, *J. Geophys. Res.*, *106*(D20), 24,051–24,062, doi:10.1029/2001JD000545.

McKenzie, R. L., C. Weinreis, P. V. Johnston, B. Liley, H. Shiona, M. Kotkamp, D. Smale, N. Takegawa, and Y. Kondo (2008), Effects of urban pollution on UV spectral irradiances, *Atmos. Chem. Phys.*, *8*, 5683–5697.

McKinley, A. F., and B. L. Diffey (1987), A reference action spectrum for ultraviolet induced erythema in human skin, in *Human Exposure to Ultraviolet Radiation: Risks and Regulations*, edited by W. R. Passchier and B. F. M. Bosnjakovic, pp. 83–87, Elsevier, Amsterdam.

Micheletti, M. I., R. D. Piacentini, and S. Madronich (2003), Sensitivity of biologically active UV radiation to stratospheric ozone changes: Effects of action spectrum shape and wavelength range, *Photochem. Photobiol.*, *78*, 456–461.

Newman, P. A., et al. (2009), What would have happened to the ozone layer if chlorofluorocarbons (CFCs) had not been regulated?, *Atmos. Chem. Phys.*, *9*, 2113–2128.

Pucai, W., and J. Lenoble (1996), Influence of clouds on UV irradiance at ground level and backscattered exittance, *Adv. Atmos. Sci.*, *13*, 217–228, doi:10.1007/BF02656864.

Seckmeyer, G., A. Bias, G. Bernhard, M. Blumthaler, C. R. Booth, K. Lantz, R.L. Mckenzie, P. Disterhoft, and A. Webb (2005), Instruments to measure solar ultraviolet radiation, Part 2: Broadband instruments measuring erythemally weighted solar irradiance, *WMO TD-1289*, World Meteorol. Org., Geneva.

Setlow, R. B. (1974), The wavelengths in sunlight effective in producing skin cancer: A theoretical analysis, *Proc. Natl. Acad. Sci. U. S. A.*, *71*(9), 3363–3366.

Stolarski, R. S., and S. Frith (2006), Search for evidence of trend slowdown in the long-term TOMS/SBUV total ozone data record: The importance of instrument drift uncertainty and fingerprint detection, *Atmos. Chem. Phys. Discuss.*, *6*, 3883–3912.

Stolarski, R. S., R. D. McPeters, and J. R. Herman (1991), Total ozone trends deduced from Nimbus 7 TOMS data, *Geophys. Res. Lett.*, *18*, 1015–1018, doi:10.1029/91GL01302.

Tanskanen, A., et al. (2007), Validation of daily erythemal doses from Ozone Monitoring Instrument with ground-based UV measurement data, *J. Geophys. Res.*, *112*, D24S44, doi:10.1029/2007JD008830.

World Meteorological Organization (WMO) (1999), Scientific assessment of ozone depletion: 1998, *Global Ozone Res. and Monit. Proj. Rep. 44*, Geneva.

World Meteorological Organization (WMO) (2003), Scientific assessment of ozone depletion: 2002, *Global Ozone Res. and Monit. Proj. Rep. 47*, Geneva.

World Meteorological Organization (WMO) (2007), Scientific assessment of ozone depletion: 2006, *Global Ozone Res. and Monit. Proj. Rep. 50*, Geneva.

J. R. Herman, NASA Goddard Space Flight Center, Greenbelt, MD 20771, USA. (jay.r.herman@nasa.gov)